Int. J. Electrochem. Sci., 16 **(2021)** Article ID: 210443, doi: 10.20964/2021.04.14

International Journal of ELECTROCHEMICAL SCIENCE
www.electrochemsci.org

PEDOT-hydroxypropyl-β-cyclodextrin Inclusion Complex as Additive for Epoxy Coating with Enhanced Anticorrosion Performance

Ligang Zhang[1,2], *Shihui Qiu*[2,*], *Bo Zhu*, *Haichao Zhao*[2,*]

[1] School of Materials Science and Engineering, Shanghai University, Shanghai 200072, China
[2] Key Laboratory of New Marine Materials and Applied Technologies, Zhejiang Key Laboratory of Marine Materials and Protective Technologies, Ningbo Institute of Materials Technology and Engineering, Chinese Academy of Sciences, Ningbo 315201, China
[*]E-mail: qiushihui@nimte.ac.cn, zhaohaichao@nimte.ac.cn

Received: 21 November 2020 / *Accepted:* 16 January 2021 / *Published:* 28 February 2021

PEDOT is a conductive polymer with a conjugated structure, which has great steric hindrance and ion exchange capacity, but its compatibility is poor. Herein, a novel PEDOT-hydroxypropyl-β-cyclodextrin (P-CD) inclusion complex was synthesized and was used as an additive for anticorrosive epoxy coating. UV, FTIR, Raman and XRD spectra demonstrated that the HP-β-CD was successfully attached with the PEDOT and enhanced the solubility and dispersion of PEDOT. The epoxy coatings without and with a small content of P-CD (0.5 wt.%, 1 wt.%) were prepared and the anticorrosion properties were assessed by electrochemical impedance spectroscopy (EIS) and corrosion product analysis. The results indicate that the composite coating exhibits a higher impedance modulus compared to the pure epoxy coating. The main reason is the barrier performance of P-CD, which increases the diffusion path of corrosive media, and P-CD can enhance corrosion resistance by promoting the formation of Fe_3O_4 passivation layer on the surface of steel.

Keywords: PEDOT; HP-β-CD; Host-guest inclusion compounds; Anticorrosion

1. INTRODUCTION

Conducting polymers (CPs) have attracted widespread attention due to their potential applications in the field of organic solar cells[1, 2], supercapacitors[3, 4], biomaterials[5], electrostatic coatings[6]. Since the 1980s, a lot of researches have been conducted by using conductive polymers for metal anticorrosion applications[7, 8]. Generally, two main methods can be adopted for the preparation of CPs-based anticorrosive coatings. One strategy is direct electrodeposition of the conductive polymer onto the metal substrate. And the other is mixing the conductive polymer into the organic coating matrix to form a composite coating. In this case, organic coating after adjunction a low concentration of CPs has been shown to impart enhanced corrosion resistance than unmodified coatings[9, 10]. However, unsubstituted or undoped conducting polymers are usually difficult to process. For the second strategy, the solubility or dispersibility of conductive polymers in the coating is critical. A lot of studies on the preparation of soluble CPs[11, 12] or dispersible CPs particles[13, 14] or nanofibers[15] for the anticorrosion application have been reported.

Among all the conducting polymers, Poly(3,4-ethylenedioxythiophene) (PEDOT) is considered the most stable CP currently[16]. However, PEDOT is known to be insoluble and infusible in most organic solvents. In 1991, Bayer of Germany synthesized a stable PEDOT/PSS colloidal dispersion with water-soluble poly (p-styrene sulfonic acid). Recently, some articles using PEDOT/PSS to prepare organic anticorrosive composite coatings have been reported. Hou et al.[17] investigated the corrosion behavior of PEDOT/PSS-coating. Results indicated that the epoxy resin containing a small amount of PEDOT/PSS revealed a better anti-corrosion performance than unmodified ones. Su et al. [18]prepared PEDOT:PSS-graphene composite coating and found that the addition of PEDOT:PSS-graphene could promote the formation of passivation layers on the surface of steel, and inhibited the corrosion reaction from further occurring. Du et al. [19] prepared LDH/PEDOT:PSS@RGO hybrid and the corresponding polyvinyl butyral−based composite coating exhibited significant corrosion resistance. But actually, PSS is acidic and corrosive to the metal matrix to a certain extent. Besides, PEDOT/PSS is hydrophilic and insoluble in oily resin, which limits its application. To address this issue, Ma et al.[20] synthesized a novel solution-processable dibutyl-substituted poly(3,4-propylenedioxythiophene) (Poly(ProDotBu$_2$)) by Grignard metathesis (GRIM) polymerization. And then UV-cured urethane acrylate coatings (PUA) with different contents of Poly(ProDotBu$_2$) were applied on Q235 carbon steel substrate. The composite organic coatings manifested good corrosion resistance and barrier properties in comparison with pure PUA coating.

β-Cyclodextrin (abbreviated as β-CD), a macromolecule containing 7 D-glucopyranose units, is widely applied in the preparation of inclusion complexes of various compounds [21-23]. Many reports have pointed out that, compared with compounds without CD, compounds containing CD exhibit significant improvements in solubility, surface morphology characteristics and reduced aggregation tendency[22-28]. In this experiment, the soluble PEDOT-hydroxypropyl-β-cyclodextrin (P-CD) inclusion complex was synthesized and the anticorrosion properties of the epoxy coating containing a small content of the complexes (0.5 wt.% and 1 wt.%) were evaluated by electrochemical impedance spectroscopy (EIS), and corrosion product analysis. After analysis, we find that P-CD coating can inhibit the corrosion of carbon steel in salt water.

2. EXPERIMENT SECTION

2.1 Materials

3,4-ethylenedioxythiophene (EDOT), hydroxypropyl-β-cyclodextrin (HP-β-CD), iron p-toluenesulfonate (Fe(OTs)$_3$) were from Aladdin Industrial Corporation. Epoxy resin and curing agent (D230 polyamide hardener) were from Shenyang Baichen Chemical Technology Co. Ltd and Aladdin

Industrial Corporation, respectively. Q235 carbon steels (1 × 1 × 1 cm^3) were polished using 400, 800 and 1200-grit sandpapers and ultrasonic treating in ethanol. Anhydrous ethanol was purchased from Sinopharm Chemical Reagent Co. Ltd. and deionized water was employed in the whole experiment.

2.2. Synthesis of P-CD complex

In a typical experiment, solution A was first prepared by dissolving 20 mmol 3,4-ethylenedioxythiophene (EDOT) and 10 mmol HP-β-CD in a mixed solution of water and methanol (20 mL:30 mL). On the other side, 20 mmol iron p-toluenesulfonate was dissolved into water and methanol (10 mL:15 mL) to prepare solution B. After then, both solution A and B were sonicated for 10 minutes. While stirring the solution A, the B solution was slowly dropping in, then the reaction started at 75 °C and lasted for 48 h. After the reaction is completed, it is dialyzed with a 2000 MW dialysis bag until the reactants and impurities no longer precipitate, leaving the reaction product with a molecular weight greater than 2000. After dialysis, the solution in the dialysis bag was centrifuged (the solvent is centrifuged out) to obtain a high concentration slurry. At last, the slurry was freeze-dried with a freeze dryer to obtain a black powder namely PEDOT: hydroxypropyl-β-cyclodextrin (P-CD). The reaction schematic diagram is shown in Scheme 1.

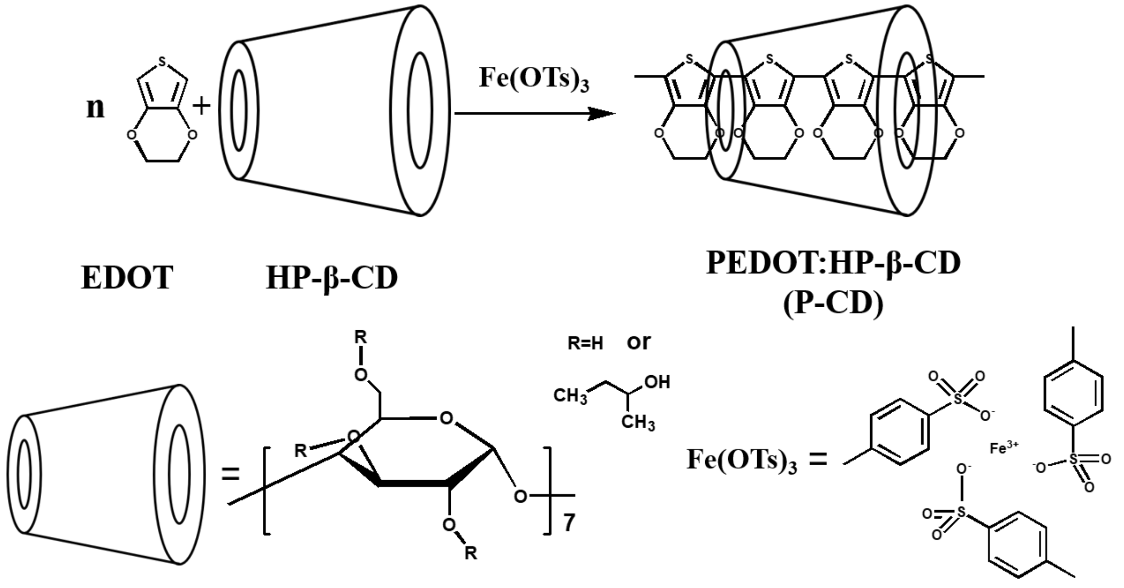

Scheme 1. Schematic diagram of the fabrication of P-CD

2.3. Preparation of composite anti-corrosion coatings

Before coating, Q235 electrodes (1 cm^2) were sanded with 400, 800, and 1200 mesh sandpapers and rinsed with deionized water. After ultrasonically removing surface grease and other substances with ethanol, electrodes were dried under nitrogen and then saved in a vacuum oven. The high concentration P-CD slurry was mixed fully with the pre-calculated epoxy resin via mechanical agitation, and then removed residual solvent with a rotary evaporator. With the curing agent (epoxy: curing agent=5:1) added, the compound was mixed entirely under the ultrasonic treating for 2 minutes, then degassed in a vacuum furnace for 5 minutes. The slurry was applied to the electrode surface with a wire rod, and the sample was cured at room temperature for three days. Then 1%P-CD coatings and 0.5%P-CD coatings were fabricated in the similar procedure, which represent the content of P-CD slurry is 1 wt.% and 0.5 wt.%. Pure epoxy coatings (EP) were also prepared without P-CD added. The thickness of the coating measured with a thickness gauge (FY20θ50) is 80±5μm.

2.4. Characterization

The physical properties of P-CD complexes were characterized by UV-vis spectroscopy (Lambda 950) and Raman spectroscopy (Renishaw in Via Reflex). Fourier transform infrared (FTIR) spectrum was applied to investigate the structure of P-CD complex, EDOT, HP-β-CD from 400 to 4000 cm^{-1}. X-ray diffractometer (XRD, Bruker D8 Advance) was applied to investigate the crystal characteristics of HP-β-CD and P-CD complex using $Cu_{K\alpha}$ (λ=0.154 nm) radiation with 2θ ranging from 5° to 60°. The surface morphology and distribution of the P-CD complex was observed by scanning electron microscopy (HITACHI S4800). The cross-section of coatings and the steel surface after corrosion were observed by field emission scanning electron microscopy (SEM, Quanta 250). The arithmetic mean deviation (Sa) for rust regions is analyzed by 3D optical profilometer (UP-Lambda). The composition of the corrosion product is characterized by Raman spectroscopy.

2.5. Electrochemical experiments

Three-electrode system of the electrochemical workstation (CHI-660E, Chenhua, Shanghai) was applied to measure the electrochemical impedance spectroscopy (EIS) of coatings in 3.5 wt.% NaCl solution, consisting of the working electrode, a saturated calomel electrode (SCE) as the reference electrode, and a platinum sheet as counter electrode. After a while, the open circuit potential (OCP) curve was steady and this value was recorded to measure the impedance of coating. The EIS measurements were performed carried out over a frequency range of 10^5 Hz to 0.01 Hz with an amplitude of 20 mV at steady open circuit potential, and the EIS results were fitted via ZSimpWin software.

3. RESULTS AND DISCUSSION

3.1. Characterization of P-CD inclusion complex

The UV-vis spectrum of P-CD complexes after polymerization is shown in Figure 1(a). The absorption band near 600 nm is attributed to *π-π** of PEDOT main chain[29], confirming the successful synthesis of PEDOT. The FTIR spectra of HP-β-CD, EDOT and P-CD complexes are shown in Figure 1(b). The purple line shows the characteristic peaks of EDOT at 3112 and 892 cm^{-1} (stretching and bending vibrations of –CH thiophene ring), 1487 and 1367 cm^{-1} (C=C and C–C stretching), 2982, 2924 and 2873 cm^{-1} (stretching vibrations of –CH, $–CH_2O$ in the ethylenedioxy group), and 934 and 761 cm^{-1} (C–S). All of these characteristic peaks have been similarly reported in other articles[14, 30]. The sharp absorption peak at 892 cm^{-1} is assigned to C-H bending vibration on the EDOT thiophene ring disappears, which proves the α, α′ coupling between the EDOT thiophene rings and the formation of the PEDOT chain[30]. Furthermore, the peaks around 2930 and 3400 cm^{-1} of HP-β-CD[31] are reflected in the P-CD complex peak, proving that HP-β-CD is grafted on PEDOT. Therefore, with the peak at 892 cm^{-1} disappearing and the peaks around 2930 and 3400 cm^{-1} appearing in the P-CD curve, the P-CD complex is successfully synthesized.

The diffraction peaks of HP-β-CD and P-CD complex are further evaluated by XRD measurement. As shown in Figure 1(c), there is a broad peak in the range of 15°-25° (2θ) shown in the XRD pattern of HP-β-CD, as same as other literature description[32], confirming its amorphous character. On the other hand, the P-CD complex has a broad diffraction peak near 25.9°, which is similar to that of the amorphous PEDOT[33] and does not exhibit the characteristic peaks of HP-β-CD, indicating that HP-β-CD has been successfully grafted on PEDOT, rather than a simple blend.

The P-CD structure is further determined through Raman spectra. Figure 1(d) shows the characteristic peaks of HP-β-CD at 2800-3000 cm^{-1} (symmetric and asymmetric C-H stretching vibration), 1460 cm^{-1} (C-H deformation), 1082 cm^{-1} and 1126 cm^{-1} (C-C and C-O single bond), 936 cm^{-1} (glucose ring vibration). Besides, there are some new peaks revealed in the spectrum of the PEDOT corresponding to 1560 cm^{-1} (C=C antisymmetric stretch); 1430 cm^{-1} (C=C symmetric stretch), 1370 cm^{-1} and 1270 cm^{-1} (C-C ring stretch), 1105 cm^{-1} (C-O-C deformation), 990 cm^{-1} (C-C antisymmetric stretching vibration), 704 cm^{-1} and 861 cm^{-1} (C-S-C symmetric deformation), 573 cm^{-1} (oxyethylene ring deformation), 443 cm^{-1} (the curvature of SO_2, corresponding to the sulfonate ion of iron p-toluenesulfonate)[34]. The weakening of the HP-β-CD peak and the appearance of the PEDOT peak in the Raman spectrum indicates that the PEDOT polymer has been successfully synthesized, and there are some intermolecular forces existing between PEDOT and HP-β-CD, mainly hydrogen bonding interaction.

The solubility of the P-CD is tested in different solvents (Figure 2a). The prepared P-CD complex has good solubility in DMF and DMSO, also has good dispersion in water and ethanol. The morphology of the P-CD inclusion complex is studied by SEM analysis (Figure 2b). Spheric-like particles with a diameter from hundreds of nanometers to several micrometers are observed. This facile soluble and dispersible P-CD inclusion complex is crucial for initiating its anticorrosive applications.

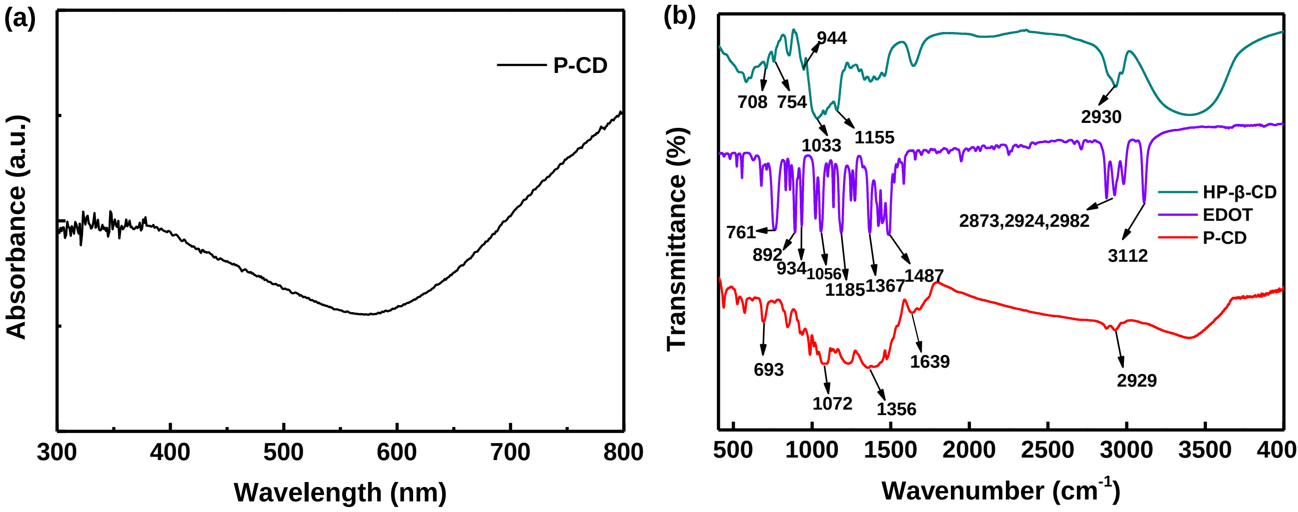

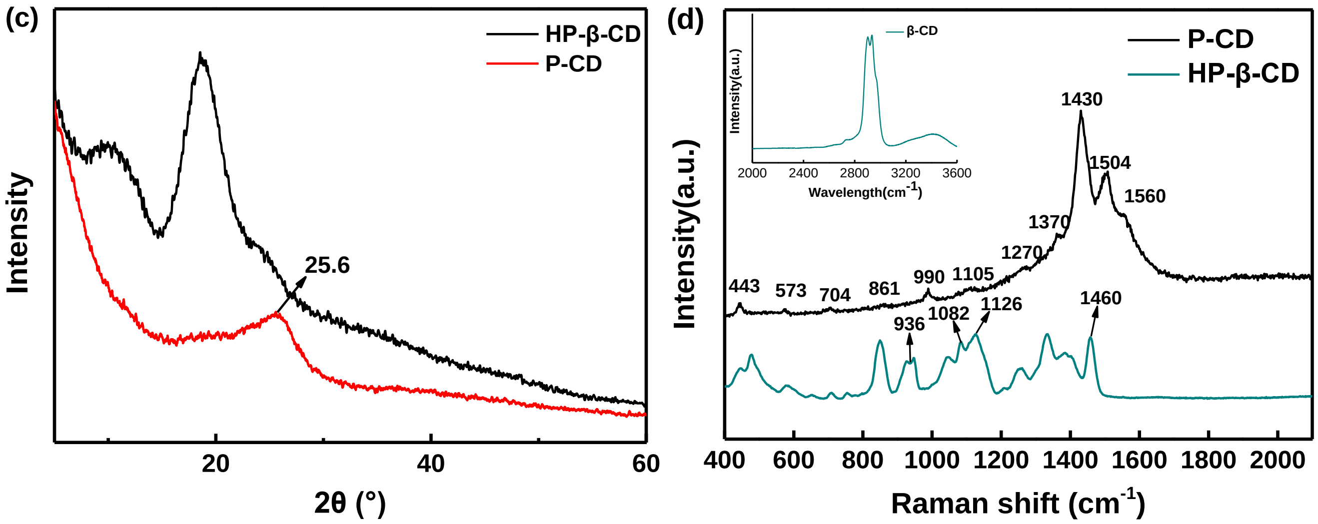

Figure 1. (a) UV-vis spectrum of P-CD complex (b) FT-IR spectra of HP-β-CD, EDOT and P-CD complex, (c) XRD patterns of HP-β-CD and P-CD complex, (d) Raman spectra of HP-β-CD and P-CD complex

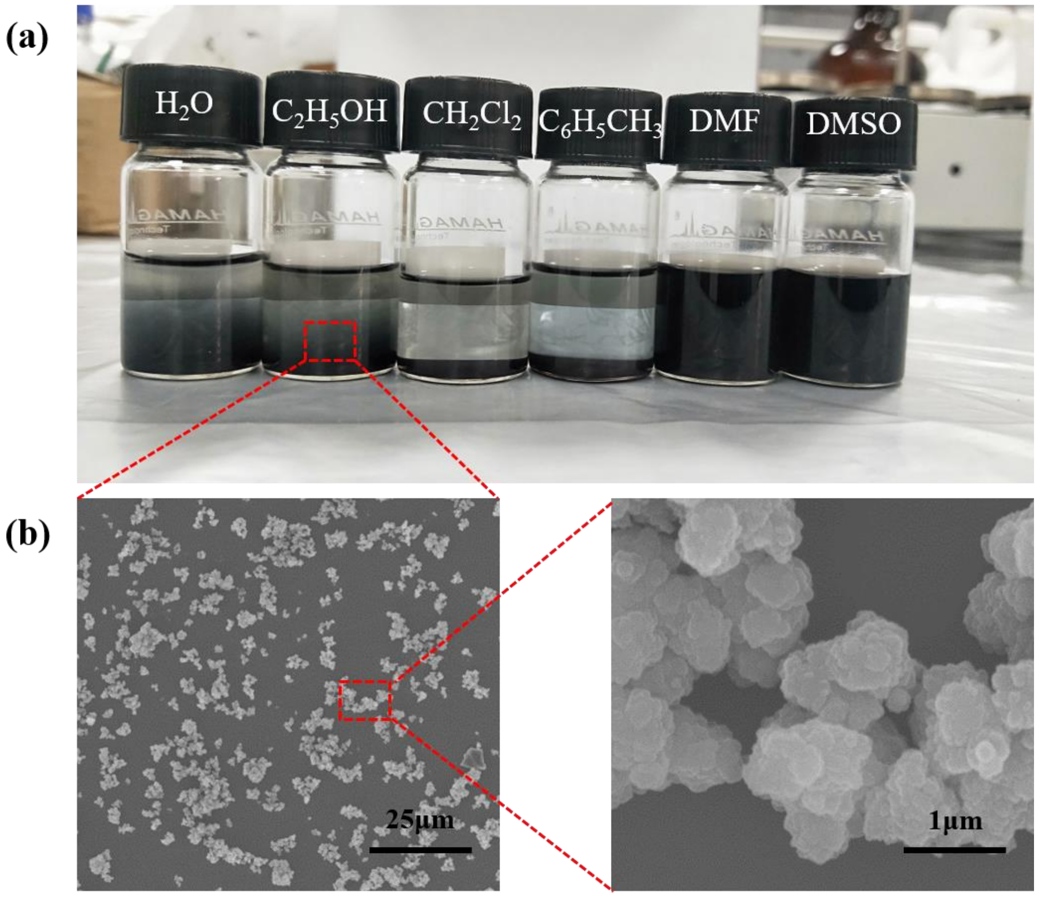

Figure 2. (a) The image of P-CD complex after 24 h dissolved in different solvents, (b) SEM images of P-CD complex

3.2 Morphology of epoxy composite coating

To evaluate the compatibility of the P-CD complex and epoxy resin, SEM is applied to observe fracture surfaces for different composite coatings. Pure epoxy exhibits a typical brittle fracture surface of thermosetting polymer[35] (Figure 3a, b). Besides, the fractured cracks are dense with some small holes. As for the 0.5%P-CD coating (Figure 3c, d), the fractured surface is relatively smooth with sparse cracks, demonstrating that 0.5%P-CD is well-dispersed in epoxy coating and obtains better compatibility. When the P-CD loading comes to 1%, obvious holes can be observed in the fracture surface, which is ascribed to the poor dispersion of P-CD (Figure 3e, f). In other words, the excess P-CD leads to obvious phase separation, resulting in an uneven and rough fractured surface.

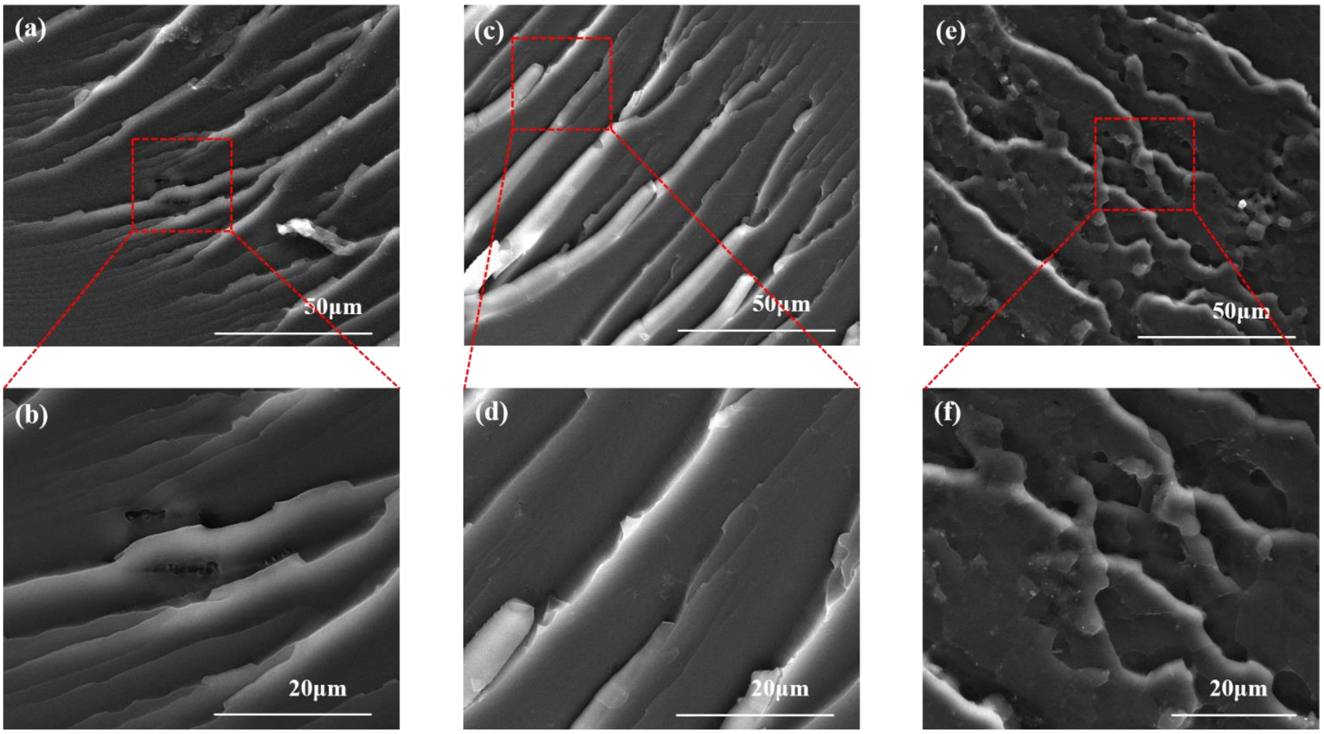

Figure 3. SEM images of the fracture surfaces for (a,b) pure-coating, (c,d) 0.5% P-CD-coating and (e,f) 1% P-CD-coating.

3.3 Electrochemical analysis

The electrochemical impedance spectra of the coatings were shown in Figure 4. The impedance modulus of the lowest frequency ($|Z|_{0.01\ \mathrm{Hz}}$) in the Bode plot is used to evaluate the barrier properties of the coating[36]. The initial $|Z|_{0.01\ \mathrm{Hz}}$ value of pure epoxy resin is $6.21\times10^{8}\ \Omega\ \mathrm{cm}^2$, and it is reduced to $6.15\times10^{7}\ \Omega\ \mathrm{cm}^2$ after soaking for 80 days, indicating that waterborne epoxy film has a weakened anti-corrosion ability with the invasion of corrosion substances. For the coating with 1%P-CD and 0.5%P-CD, the initial $|Z|_{0.01\ \mathrm{Hz}}$ value are $1.87\times10^{9}\ \Omega\ \mathrm{cm}^2$ and $2.20\times10^{9}\ \Omega\ \mathrm{cm}^2$ respectively, which are higher than that of pure epoxy resin ($6.21\times10^{8}\ \Omega\ \mathrm{cm}^2$). Over 80 days of immersion, the $|Z|_{0.01\ \mathrm{Hz}}$ values of coating with 1%P-CD and 0.5%P-CD decrease to $4.00\times10^{8}\ \Omega\ \mathrm{cm}^2$ and $4.84\times10^{8}\ \Omega\ \mathrm{cm}^2$, which are also significantly higher than that of pure epoxy coating. From the data above, it is easy to be seen that the well-dispersed P-CDs endued the epoxy coating with the enhanced barrier ability.

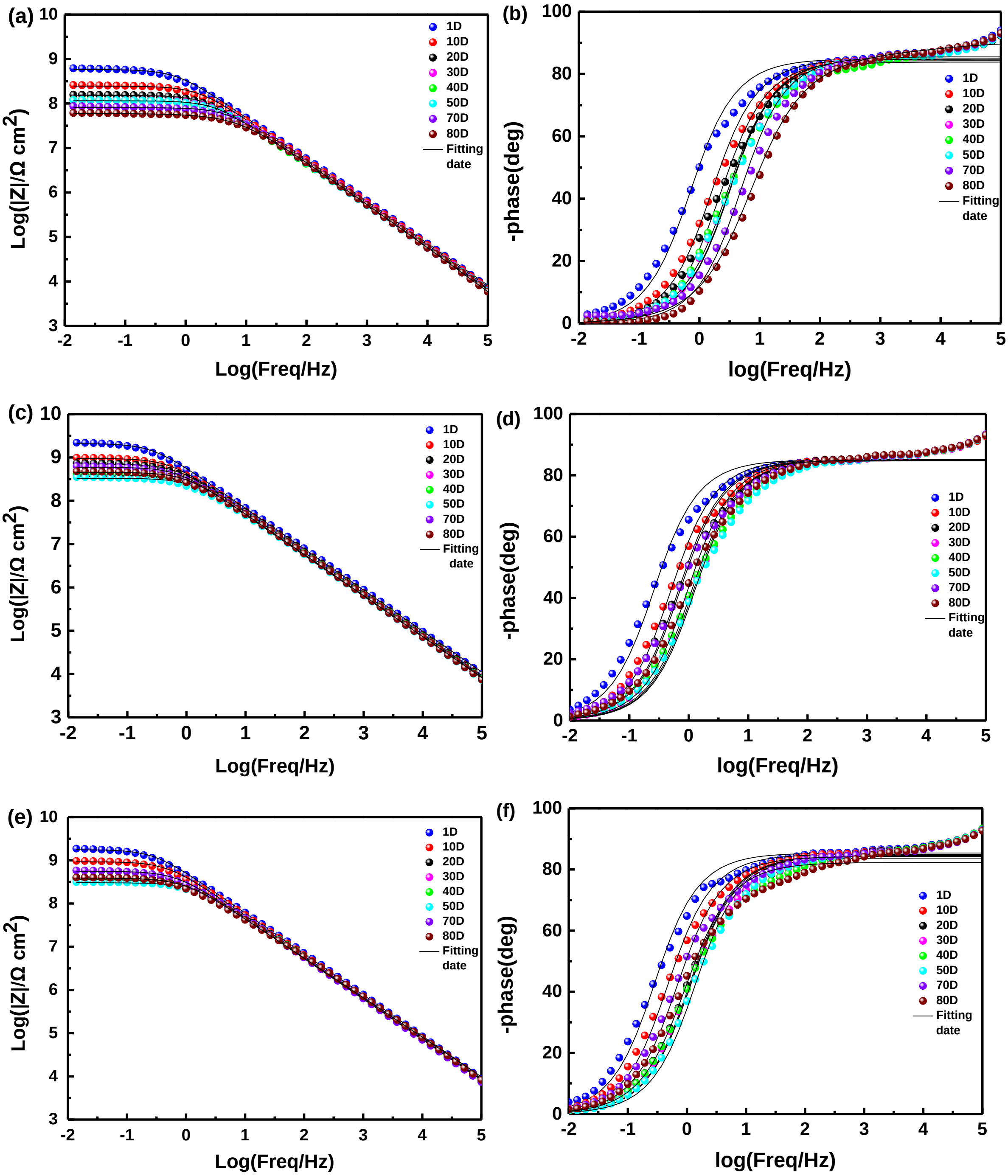

Figure 4. The electrochemical impedance spectra of (a, b) pure-coating, (c, d) 0.5%P-CD-coating and (e, f) 1%P-CD-coating.

Besides, the frequency value for the phase angle at -45°, also called the breakpoint frequency (f_b) usually reflects the microscopic delaminated regions between the steel substrate and coatings [37, 38].

It is positively correlated with the degree of coating delamination and negatively correlated with anti-corrosion [39]. As shown in Figure 5a, the f_b for 1%P-CD and 0.5%P-CD samples are similar and didn't increase, which means the interfacial adhesion of coatings is still high and coatings haven't started to delaminate. The f_b of pure coating exhibits an increased tendency with the prolonging of immersion. This is ascribed to the corrosion reactions at the interface of coating and metal, resulting in the generation of corrosive products. And f_b of pure coating was much higher than 0.5%P-CD and 1%P-CD after 10 days of immersion, showing that the coating hardly resists the penetration of corrosion medium and there are more delaminated regions on the interface between steel and coating. The composite coating with a P-CD content of 0.5% shows a stable or even a small decline in f_b after being soaked for 50 days, indicating that it can effectively delay the delamination of the coating in the salt solution.

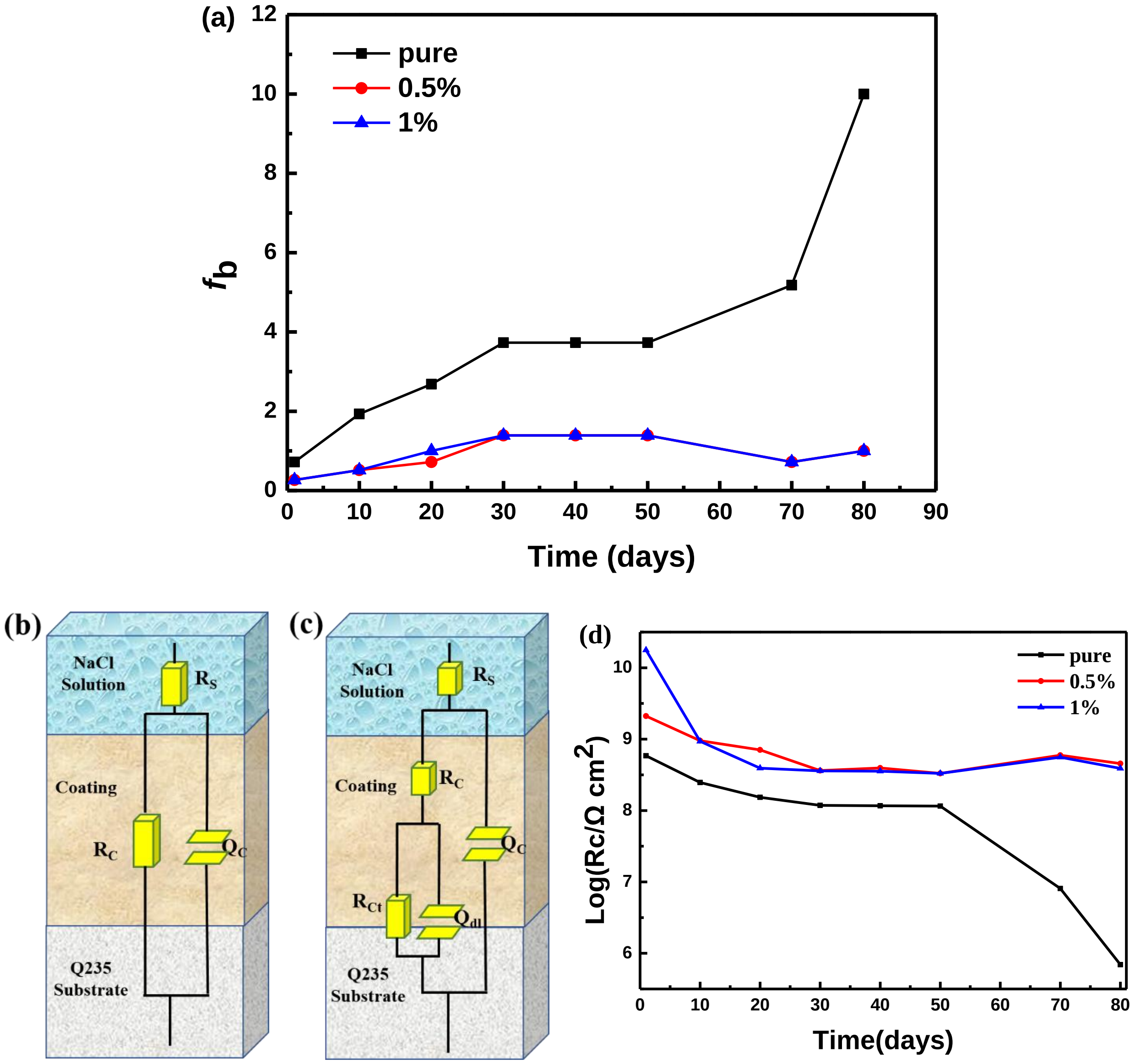

Figure 5. (a) The variation of f_b with the immersion days, (b-c) Electrical equivalent circuit models, (d) Evolution of Rc with immersion in 3.5 wt.% NaCl solution.

To further investigate electrochemical behavior, we simulate the electrochemical equivalent circuit by using ZSimpWin 3.30 software. The equivalent circuit diagram of the pure coating after 50 days immersion is shown in Figure 5c, indicating that the corrosion reaction has occurred in the electrode surface. And Figure 5b depicts the equivalent circuit diagram of the P-CD coatings, indicating that the barrier effect of the coating has not been invalid. The electrical equivalent circuit is composed of Rc, Rs and Qc, which represented coating resistance, solution resistance and coating capacitance, respectively. And coating resistances describe the barrier properties of the coatings [10]. R_{ct} (charge transfer resistance) and Q_{dl} (electric double layer capacitance) will appear when the coating is corroded and damaged by corrosive ions, water and oxygen.[40, 41]. The charge transfer resistance is usually used to describe the degree of charge transfer between the metal and the coating, which is inversely proportional to the corrosion rate of the metal. R_c value decreases with the immersion time increased, which indicates that the corrosion reaction under the coating is underway. Corrosive electrolytes and water gradually diffuse to the steel surface through cracks or pores of the coating and cause severe metal corrosion. Figure 5d shows the evolution of R_c with immersion in 3.5 wt.% NaCl solution. It is not difficult to see that the Rc of all samples shows a downward trend, indicating that the coating is being gradually corroded by corrosive substances, and then penetrates the surface of the metal substrate. However, within the time range of 50-80 days, the Rc of the coating with P-CD stabilized, which is in sharp inverse proportion to the straight decline of the pure coating. After comparison, it is found that the 0.5%P-CD coating exhibits the highest resistance because the addition of PEDOT plays a good dispersion effect and improves the barrier property of the coating.

3.4 Analysis of corrosion products

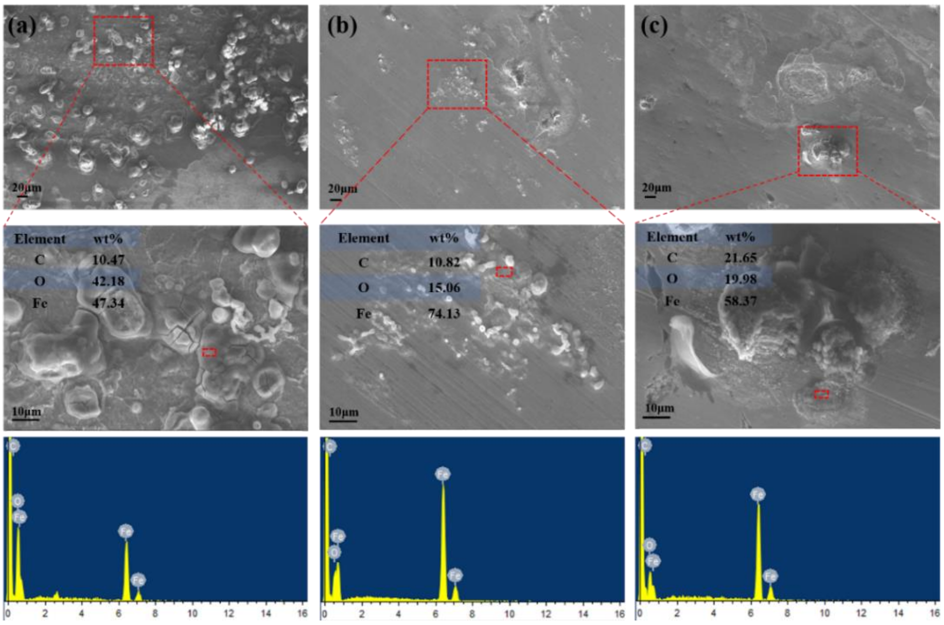

Figure 6. SEM images and EDS spectra for rust regions on the Q235 steel substrate beneath (a) pure-coating, (b) 0.5% P-CD-coating and (c) 1% P-CD-coating.

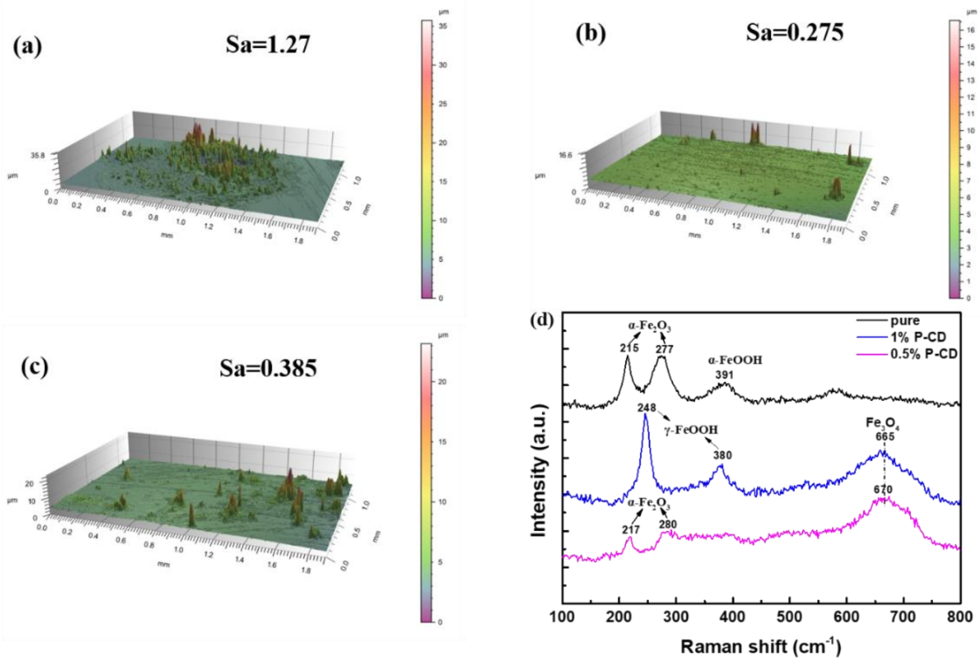

Figure 7. The arithmetic mean deviation (Sa) and the 3D micro morphology for rust regions on the steel substrate beneath (a) pure-coating, (b) 0.5% P-CD-coating and (c) 1% P-CD-coating, (d) Raman spectra of the rust regions on the steel substrate beneath pure, 0.5% P-CD-coating, and 1% P-CD-coating.

The corrosion products beneath the coating without and with P-CD after 80d immersion are observed by SEM as shown in Figure 6. The area of corrosion products under the pure coating sample (Figure 6a) is large and concentrated, indicating that the metal substrate is corroded seriously. On the contrary, the corrosion product of the P-CD containing coatings are relatively scattered, showing a small area spread, some parts are better wrapped by corrosion products. Besides, from the EDS dates, the P-CD containing coatings exhibits much lower oxygen content (15.06% and 19.98%) compared to that of pure epoxy coating (42.18%), reflecting their better anti-corrosion performance.

The roughness of the rust region described by the arithmetic mean deviation (Sa) and the 3D micromorphology for rust regions on the steel substrate are shown in Figure 7. It's not difficult to find that the rust region beneath 0.5% P-CD coating is smoother and shows the lowest Sa value, indicating that it is less corroded. Figure 7d shows the Raman spectra of the corrosion products of pure epoxy resin consisted of α-Fe_2O_3 (215 cm^{-1}, 277 cm^{-1}) and α-FeOOH (391 cm^{-1}); the corrosion products of 1% P-CD-coatings are composed of γ-FeOOH (248 cm^{-1}, 380 cm^{-1}), and Fe_3O_4 (665 cm^{-1}). Besides, it is obvious that the corrosion products of coatings containing 0.5% P-CD are mainly composed of Fe_3O_4 (670 cm^{-1}) [42, 43], indicating the passivation film formation, which isolates Fe from external solutions and air, and protects metals from corrosion.

4. CONCLUSION

In this paper, the PEDOT-hydroxypropyl-β-cyclodextrin (P-CD) inclusion complex is prepared via the oxidative polymerization method, and the anti-corrosion effect of P-CD on anticorrosion behavior of waterborne epoxy coating is studied. The results show that P-CD is well integrated into the epoxy coating and play a positive role in corrosion protection through the barrier effect and the formation of the passivation layer of Fe_3O_4. In contrast with pure epoxy coating, it indicates that epoxy coating containing a small amount of P-CD (0.5 wt.%) possesses superior corrosion protection performance. This P-CD inclusion complex could provide new routes to prepare waterborne organic coatings with enhanced anticorrosion applications.

References

1. S. Guenes, H. Neugebauer, N. S. Sariciftci, *Chem. Rev.*, 107 (2007) 1324-1338.
2. S. Sakurai, Y. Kawamata, M. Takahash, K. Kobayashi, *Jounal of oleo science*, 60 (2011) 639-646.
3. S. Cho, M. Kim, J. Jang, *ACS Appl Mater Interfaces*, 7 (2015) 10213-10227.
4. Z. Zhao, G. F. Richardson, Q. Meng, S. Zhu, H. C. Kuan, J. Ma, *Nanotechnology*, 27 (2016) 042001.
5. A. C. da Silva, A. T. S. Semeano, A. H. B. Dourado, H. Ulrich, S. I. Cordoba de Torresi, *ACS Omega*, 3 (2018) 5593-5604.
6. F. Wang, L. Feng, M. Lu, *Polymers*, 11 (2019) 714.
7. D. W. DeBerry, *Journal of the Electrochemcal Society*, 132 (1985) 1022-1026.
8. G. Mengoli, M. Munari, P. Bianco, S. Musiani, *J. Appl. Polym. Sci*., 26 (1981) 4247-4257.
9. S. H. Qiu, C. Chen, M. J. Cui, W. Li, H. C. Zhao, L. P. Wang, *Appl. Surf. Sci*., 407 (2017) 213-222.
10. S. H. Qiu, W. Li, W. R. Zheng, H. C. Zhao, L. P. Wang, *Acs Applied Materials & Interfaces*, 9 (2017) 34294-34304.
11. A.Patrick, McCarthy, H. J. Yu, Y. Sze-Cheng, W. Hsing-Lin, *langmuir*, 18 (2002) 259-263.
12. S. Tarkuc, E. Sahmetlioglu, C. Tanyeli, I. M. Akhmedov, L. Toppare, *Electrochim. Acta*, 51 (2006) 5412-5419.
13. D. Eun Park, Y. Zhen Dong, H. Jin Choi, *Eur. Polym. J.*, 101 (2018) 255-261.
14. Y. Qian, T. Wang, X. Q. Qiu, D. C. Zhao, D. Liu, Y. H. Deng, *ACS Sustainable Chemistry & Engineering*, 4 (2016) 7193-7199.
15. Y. C. Yao, H. Sun, Y. L. Zhang, Z. D. Yin, *Prog. Org. Coat*., 139 (2020) 105407.
16. C. Ocampo, R. Oliver, E. Armelin, C. Alemán, F. Estrany, *Journal of Polymer Research*, 13 (2005) 193-200.
17. J. Hou, G. Zhu, J. K. Xu, H. J. Liu, *Journal of Materials Science & Technology*, 29 (2013) 678-684.
18. Y. Su, S. H. Qiu, Y. Liu, D. P. Yang, H. C. Zhao, L. P. Wang, *International Journal of Electrochemical Science*, 14 (2019) 4595-4610.
19. P. Du, J. Wang, G. Z. Liu, H. C. Zhao, L. P. Wang, *Materials Chemistry Frontiers*, 3 (2019) 321-330.
20. J. Ma, Y. F. Zhou, J. Xu, L. Gu, G. Q. Lai, B. Chen, S. Liu, H. C. Zhao, H. B. Yu, J. M. Chen, *International Journal of Electrochemical Science*, 10 (2015) 10104-10118.
21. D. Landy, I. Mallard, A. Ponchel, E. Monflier, S. Fourmentin, *Environmental Chemistry Letters*, 10 (2012) 225-237.
22. Z. Wang, F. Cui, Y. Pan, L. Hou, B. Zhang, Y. Li, L. Zhu, *Carbohydr. Polym*., 213 (2019) 352-360.
23. S. Prabu, K. Sivakumar, M. Swaminathan, R. Rajamohan, *Spectrochim. Acta Part A*, 147 (2015) 151-157.
24. A. Farcas, A. M. Resmerita, P. H. Aubert, F. Farcas, I. Stoica, A. Airinei, *Beilstein J. Org. Chem*., 10 (2014) 2145-2156.

25. A. Farcas, A.-M. Resmerita, P.-H. Aubert, I. Ghosh, S. Cantin, W. M. Nau, *Macromol. Chem. Phys.*, 216 (2015) 662-670.
26. A. Farcas, G. Tregnago, A.-M. Resmerita, S. T. Dehkordi, S. Cantin, F. Goubard, P.-H. Aubert, F. Cacialli, *J. Polym. Sci., Part A: Polym. Chem.*, 52 (2014) 460-471.
27. M. J. Frampton, H. L. Anderson, *Angew. Chem. Int. Ed.*, 46 (2007) 1028-1064.
28. D. Thomsson, R. Camacho, Y. Tian, D. Yadav, G. Sforazzini, H. L. Anderson, I. G. Scheblykin, *Small*, 9 (2013) 2619-2627.
29. J. Ouyang, Q. Xu, C.-W. Chu, Y. Yang, G. Li, J. Shinar, *Polymer*, 45 (2004) 8443-8450.
30. D. Han, G. Yang, J. Song, L. Niu, A. Ivaska, *J. Electroanal. Chem.*, 602 (2007) 24-28.
31. B. Espinosa F., G. Hernández J., *Revista Mexicana de Ciencias Farmaceuticas*, 36 (2005) 18-24.
32. J. Wang, Y. Cao, B. Sun, C. Wang, *Food Chem.*, 124 (2011) 1069-1075.
33. K.E. Aasmundtveit, E.J. Samuelsent, L.A.A. Pettersson, O. Inganas, T. Johansson, R. Feidenhans, *Synth. Met.*, 101 (1999) 561-564.
34. M. Tahir, L. He, W. A. Haider, W. Yang, X. Hong, Y. Guo, X. Pan, H. Tang, Y. Li, L. Mai, *Nanoscale*, 11 (2019) 7761-7770.
35. S. Lu, S. Li, J. Yu, Z. Yuan, B. Qi, *RSC Advances*, 3 (2013) 8915-8923
36. S. Zhou, X. Zhu, L. Ma, Q. Yan, S. Wang, *Surf. Sci.*, 677 (2018) 193-202.
37. B. Ramezanzadeh, G. Bahlakeh, M. Ramezanzadeh, *Corros. Sci.*, 137 (2018) 111-126.
38. B. Ramezanzadeh, S. Niroumandrad, A. Ahmadi, M. Mahdavian, M. H. M. Moghadam, *Corros. Sci.*, 103 (2016) 283-304.
39. Y. Su, S. H. Qiu, D. P. Yang, S. Li, H. C. Zhao, L. P. Wang, Q. J. Xue, *J. Hazard. Mater.*, 391 (2020) 122215
40. C. H. L. Weijtens, V. van Elsbergen, M. M. de Kok, S. H. P. M. de Winter, *Org. Electron.*, 6 (2005) 97-104.
41. J. W. Zhao, S. M. Xu, K. Tschulik, R. G. Compton, M. Wei, D. O'Hare, D. G. Evans, X. Duan, *Adv. Funct. Mater.*, 25 (2015) 2745-2753.
42. X. H. Nie, X. G. Li, C. W. Du, Y. Z. Huang, H. Du, *Journal of Raman Spectroscopy*, 40 (2009) 76-79.
43. X. Zhang, K. Xiao, C. F. Dong, J. S. Wu, X. G. Li, Y. Z. Huang, *Engineering Failure Analysis*, 18 (2011) 1981-1989.